Supporting Information

Luminescent Dysprosium Single-Molecule Magnets Made from Chiral BINOL-Derived Bisphosphate Ligands

Carlo Andrea Mattei,[a] Vincent Montigaud,[a] Vincent Dorcet,[a] François Riobé,[b] Gilles Argouarch,[a] Olivier Maury,[b] Boris Le Guennic,[a] Olivier Cador,[a] Claudia Lalli,*[a] Fabrice Pointillart,*[a]

[a] *Univ Rennes, CNRS, ISCR (Institut des Sciences Chimiques de Rennes) - UMR 6226, 35000 Rennes, France*

[b] *Univ Lyon, Ens de Lyon, CNRS UMR 5182, Université Claude Bernard Lyon 1, Laboratoire de Chimie, F69342, Lyon, France*

Corresponding author's email: fabrice.pointillart@univ-rennes1.fr

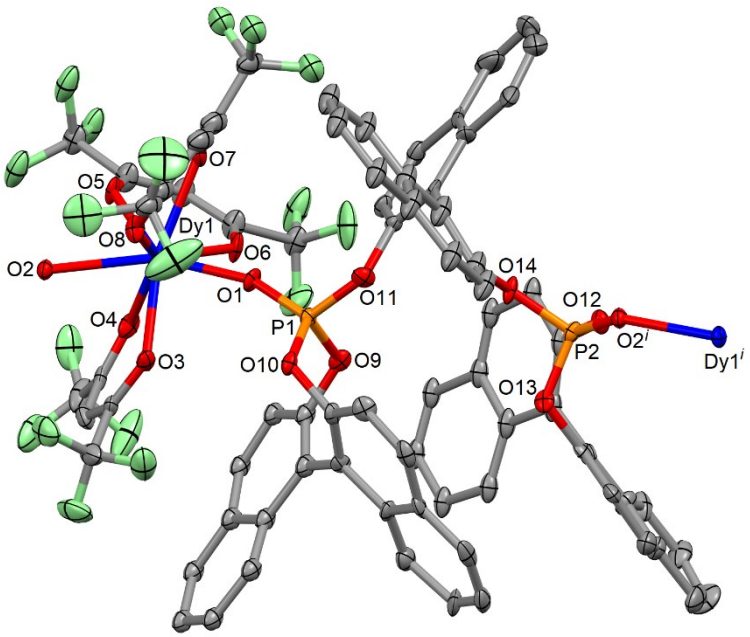

Figure S1. ORTEP view of the asymmetric unit for **[(*S*)-2]$_n$**. Thermal ellipsoids are drawn at 30% probability. Hydrogen atoms are omitted for clarity.

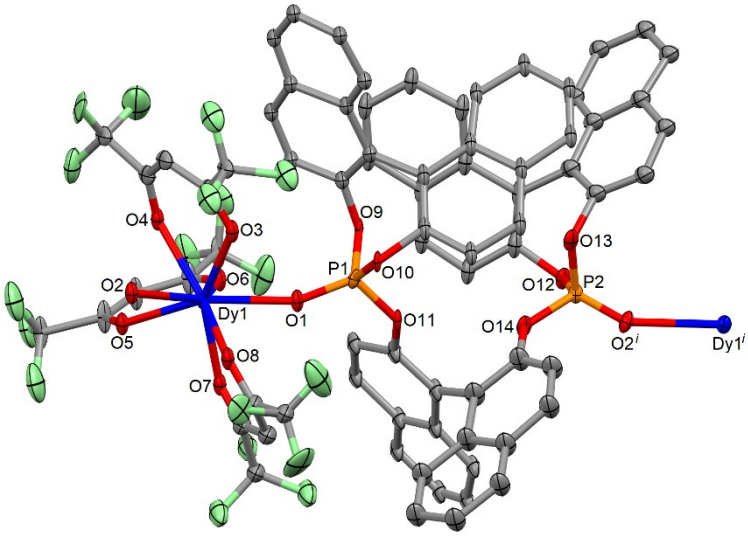

Figure S2. ORTEP view of the asymmetric unit for **[(*R*)-2]$_n$**. Thermal ellipsoids are drawn at 30% probability. Hydrogen atoms are omitted for clarity.

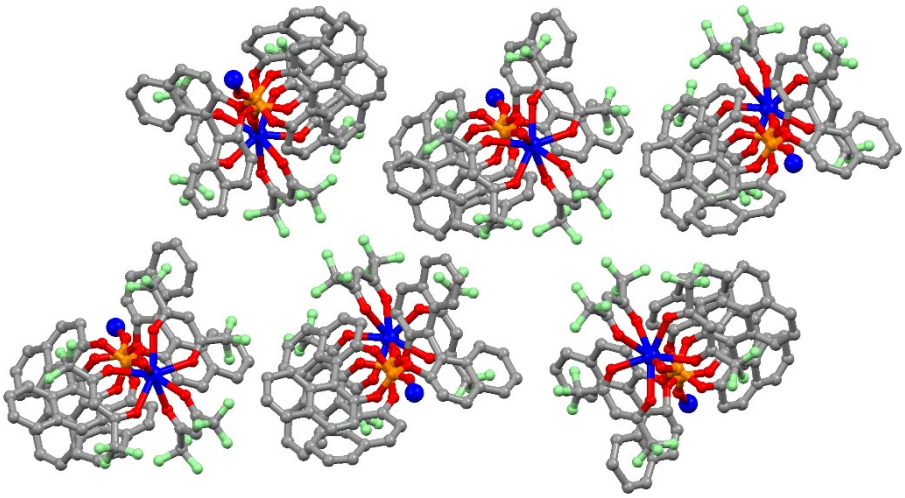

Figure S3. Crystal packing of **[(*R*)-2]$_n$** along the *c* axis.

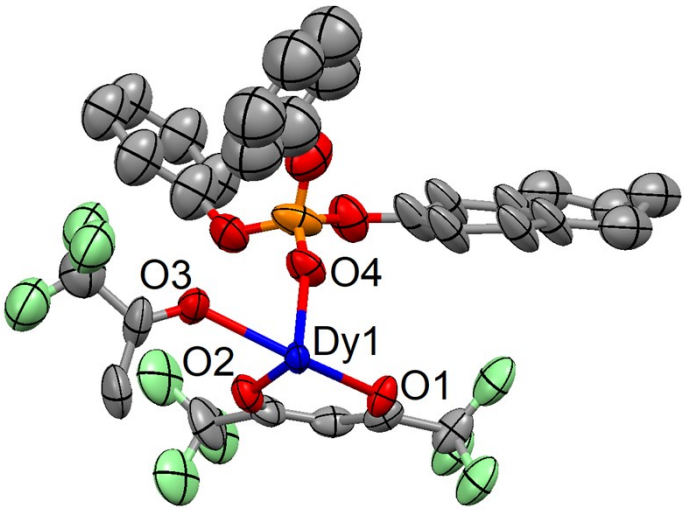

Figure S4. ORTEP view of the asymmetric unit for **[(*S*)-3]$_n$**. Thermal ellipsoids are drawn at 30% probability. Hydrogen atoms are omitted for clarity.

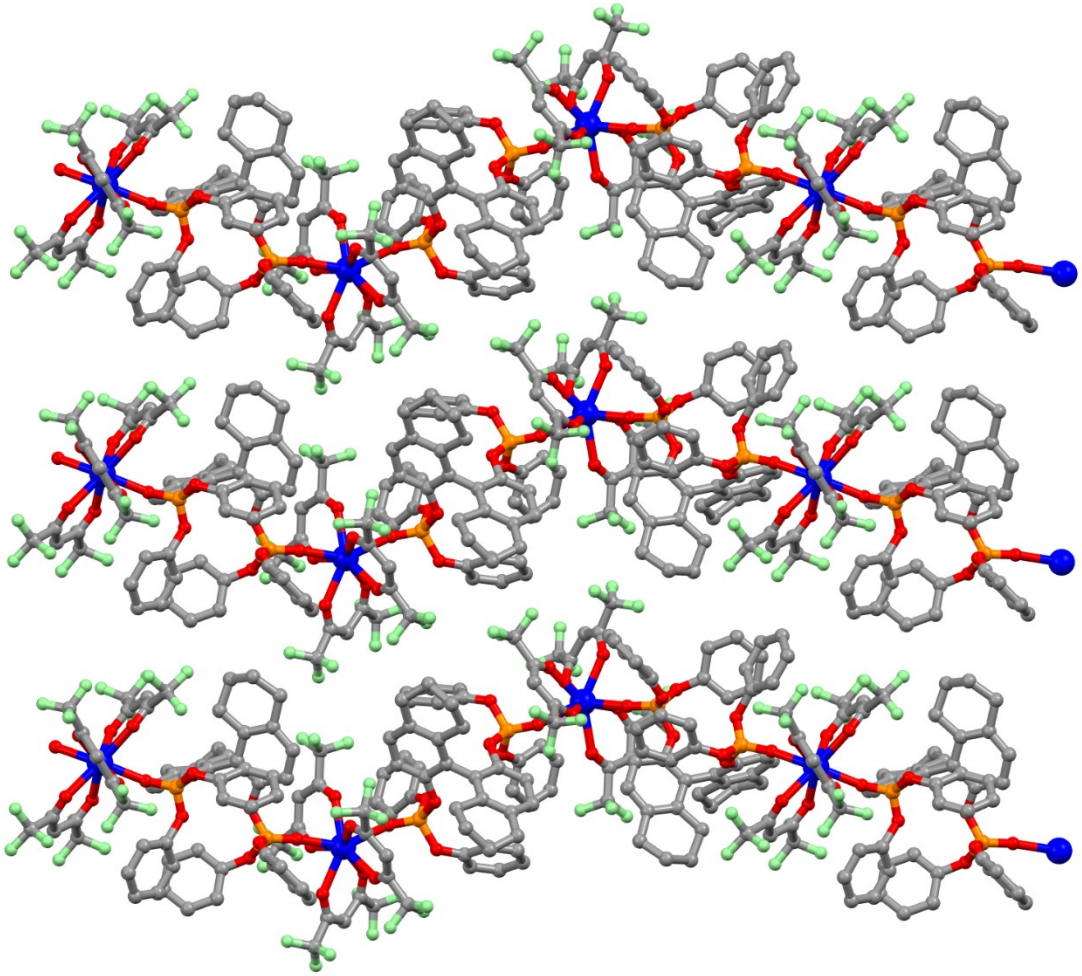

Figure S5. Crystal packing of **[(*S*)-3]$_n$** along the *c* axis.

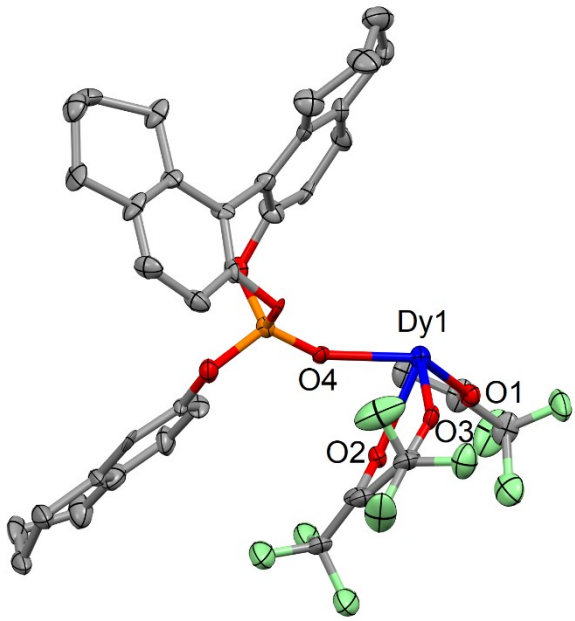

Figure S6. ORTEP view of the asymmetric unit for **[(*S*)-4]$_n$**. Thermal ellipsoids are drawn at 30% probability. Hydrogen atoms are omitted for clarity.

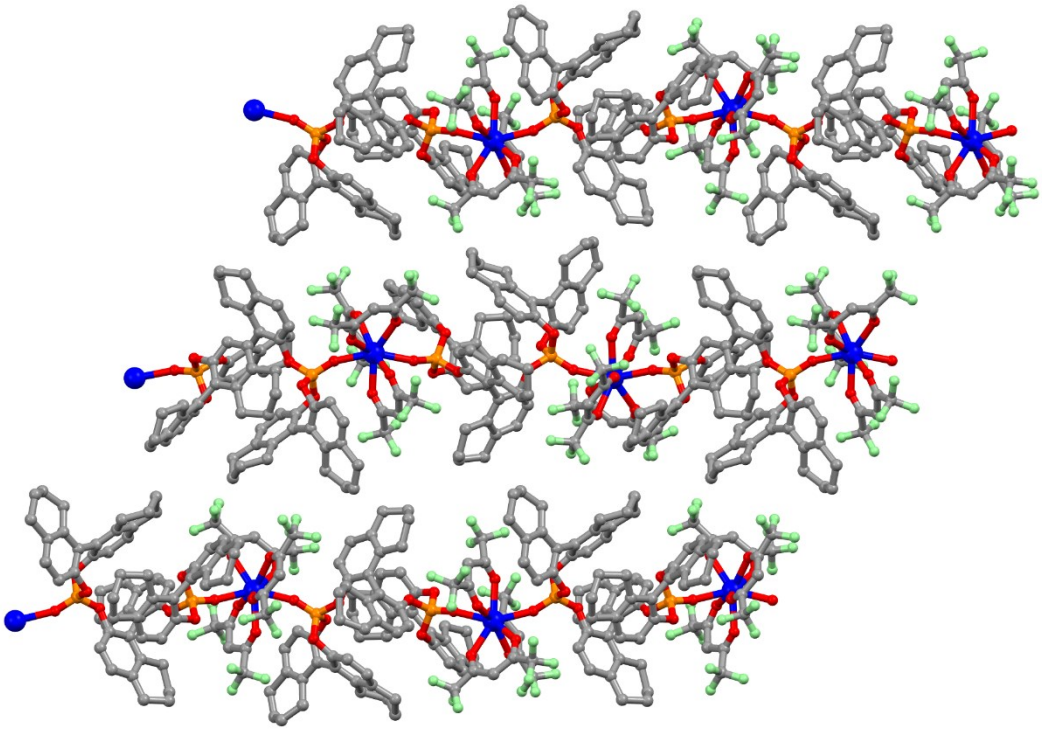

Figure S7. Crystal packing of **[(*S*)-4]$_n$** along the *c* axis.

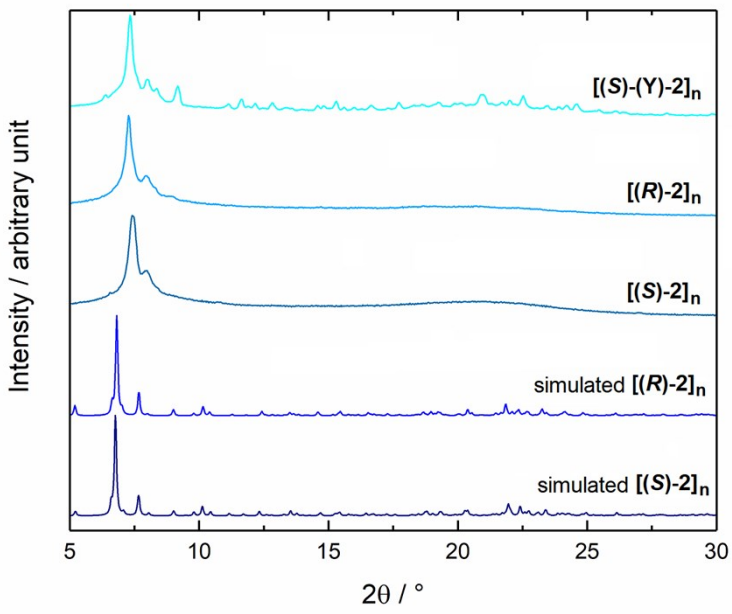

Figure S8. Superposition of experimental powder X-ray diffraction patterns from **[(*S*)-2]$_n$**, **[(*R*)-2]$_n$** and the yttrium analogue **[(*S*)-(Y)-2]$_n$** measured at 300 K and simulated from **[(*S*)-2]$_n$** and **[(*R*)-2]$_n$** single-crystal data obtained at 150 K.

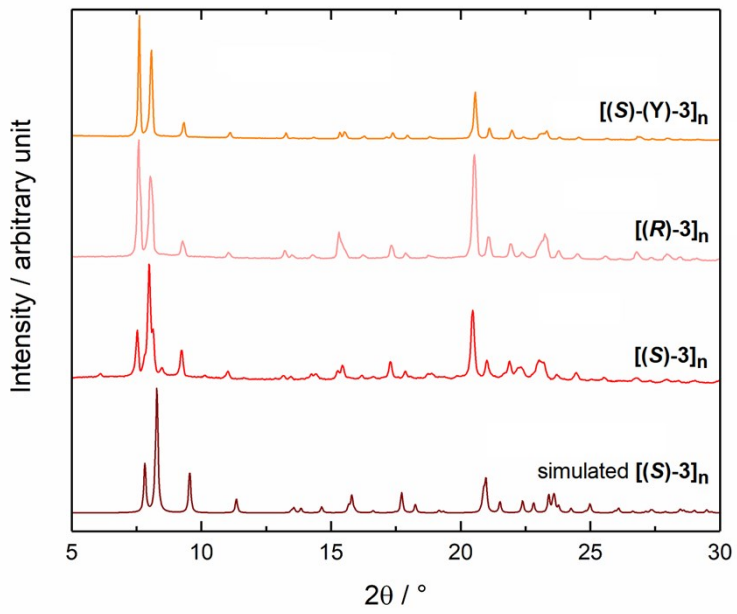

Figure S9. Superposition of experimental powder X-ray diffraction patterns from **[(*S*)-3]$_n$**, **[(*R*)-3]$_n$** and the yttrium analogue **[(*S*)-(Y)-3]$_n$** measured at 300 K and simulated from **[(*S*)-3]$_n$** single-crystal data obtained at 150 K.

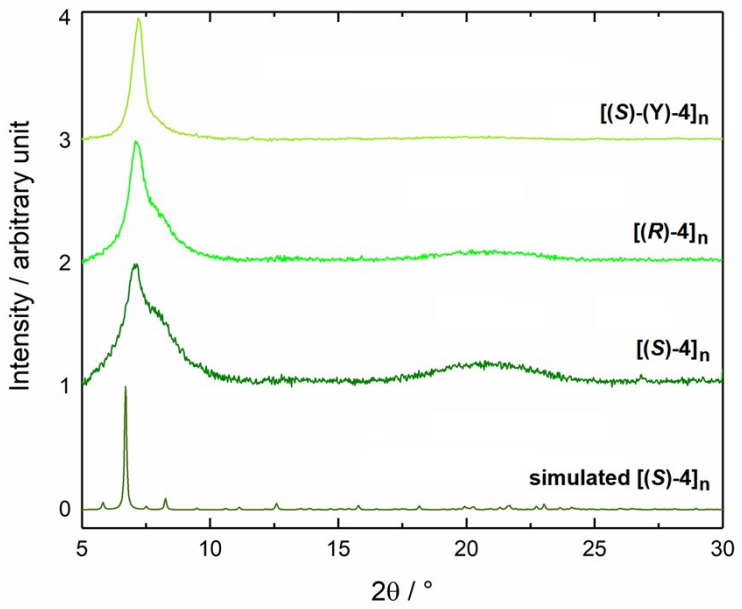

Figure S10. Superposition of experimental powder X-ray diffraction patterns from **[(*S*)-4]$_n$**, **[(*R*)-4]$_n$** and the yttrium analogue **[(*S*)-(Y)-4]$_n$** measured at 300 K and simulated from **[(*S*)-4]$_n$** single-crystal data obtained at 150 K.

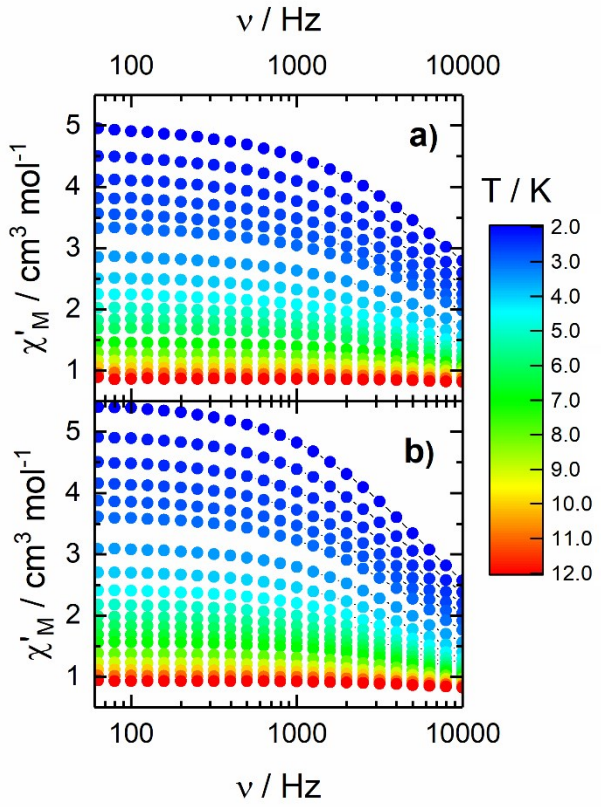

Figure S11. In phase component χ_M' of the ac magnetic susceptibility data for **[(*S*)-2]$_n$** (a) and **[(*S*)-3]$_n$** (b) from 2 to 12 K under 0 Oe.

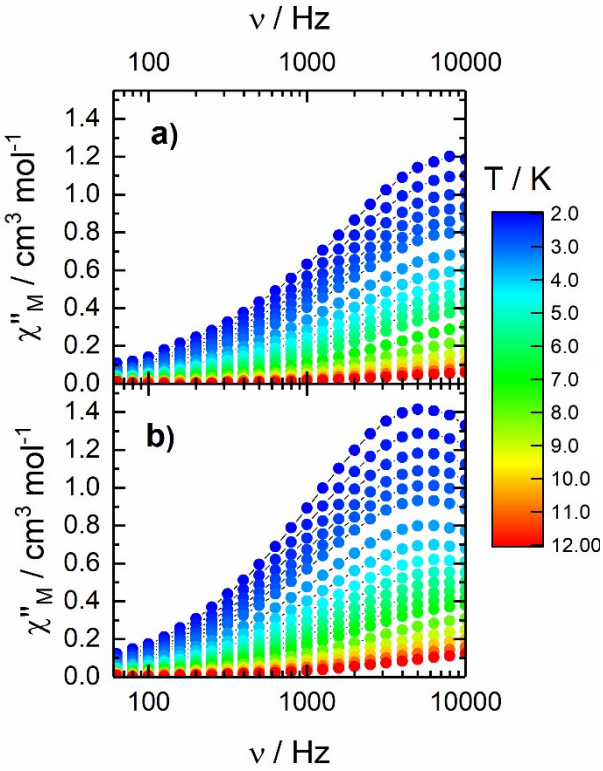

Figure 12. Out-of phase component χ_M'' of the ac magnetic susceptibility data for **[(*S*)-2]$_n$** (a) and **[(*S*)-3]$_n$** (b) from 2 to 12 K under 0 Oe.

Extended Debye model.

$$\chi_M' = \chi_S + (\chi_T - \chi_S)\frac{1+(\omega\tau)^{1-\alpha}\sin\left(\alpha\frac{\pi}{2}\right)}{1+2(\omega\tau)^{1-\alpha}\sin\left(\alpha\frac{\pi}{2}\right)+(\omega\tau)^{2-2\alpha}}$$

$$\chi_M'' = (\chi_T - \chi_S)\frac{(\omega\tau)^{1-\alpha}\cos\left(\alpha\frac{\pi}{2}\right)}{1+2(\omega\tau)^{1-\alpha}\sin\left(\alpha\frac{\pi}{2}\right)+(\omega\tau)^{2-2\alpha}}$$

With χ_T the isothermal susceptibility, χ_S the adiabatic susceptibility, τ the relaxation time and α an empiric parameter which describe the distribution of the relaxation time. For SMM with only one relaxation time, α is close to zero. The extended Debye model was applied to fit simultaneously the experimental variations of χ_M' and χ_M'' with the frequency ν of the oscillating field ($\omega = 2\pi\nu$). Typically, only the temperatures for which a maximum on the χ'' vs. *f* curves, have been considered. The best fitted parameters τ, α, χ_T, χ_S are listed in Tables S3-S10 with the coefficient of determination R^2.

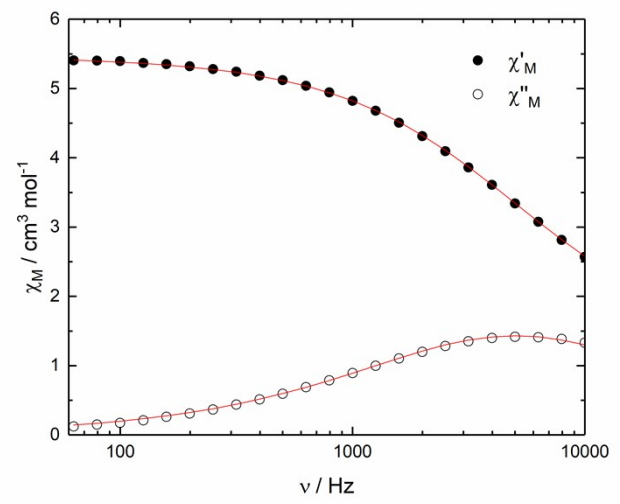

Figure S13. Frequency dependence of the in-phase (χ_M') and out-of-phase (χ_M") components of the ac susceptibility at 2 K and 0 Oe with the best fitted curves (red lines) for **[(*S*)-3]$_n$**.

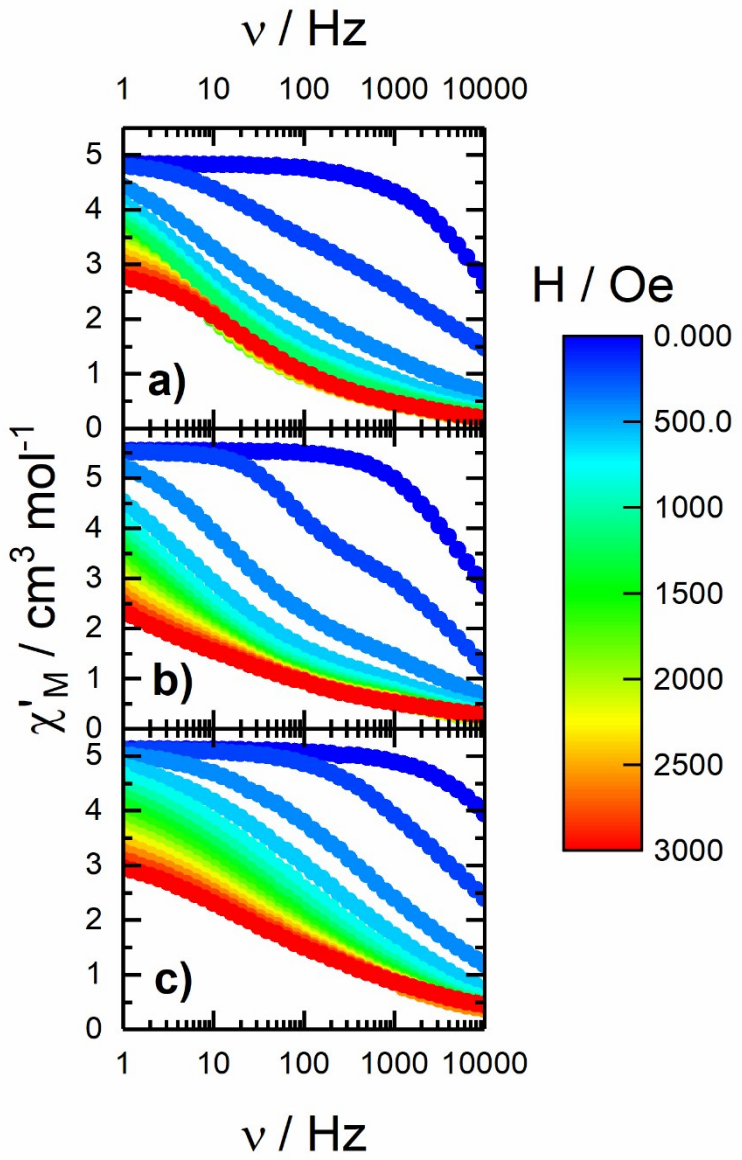

Figure S14. In-phase component of the ac magnetic susceptibility for **[(*S*)-2]$_n$** (a), **[(*S*)-3]$_n$** (b) and **[(*S*)-4]$_n$** (c) at 2 K under a DC magnetic field from 0 to 3000 Oe.

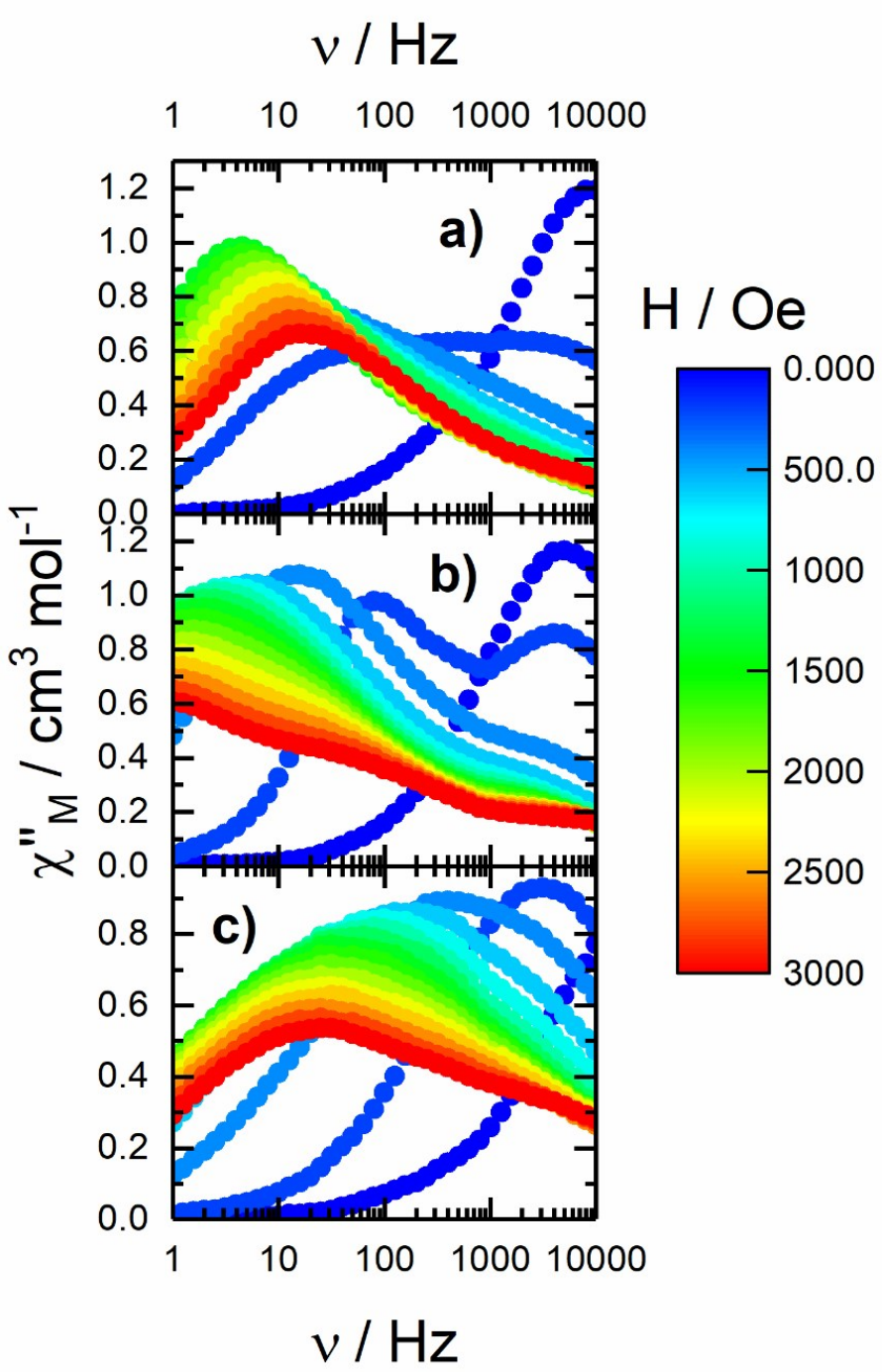

Figure S15. Out-of-phase components of the ac magnetic susceptibility for **[(*S*)-2]$_n$** (a), **[(*S*)-3]$_n$** (b) and **[(*S*)-4]$_n$** (c) at 2 K under a DC magnetic field from 0 to 3000 Oe.

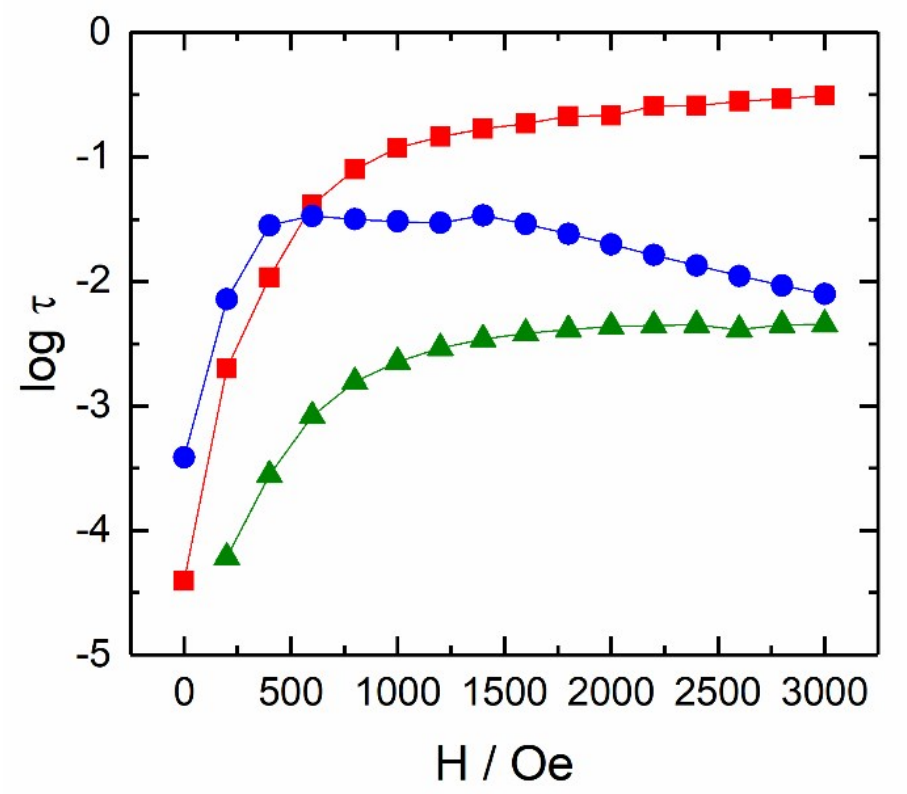

Figure S16. Field-dependence of the relaxation time of the magnetization for **[(*S*)-2]$_n$** (blue), **[(*S*)-3]$_n$** (red) and **[(*S*)-4]$_n$** (green) at 2 K under a DC magnetic field from 0 to 3000 Oe.

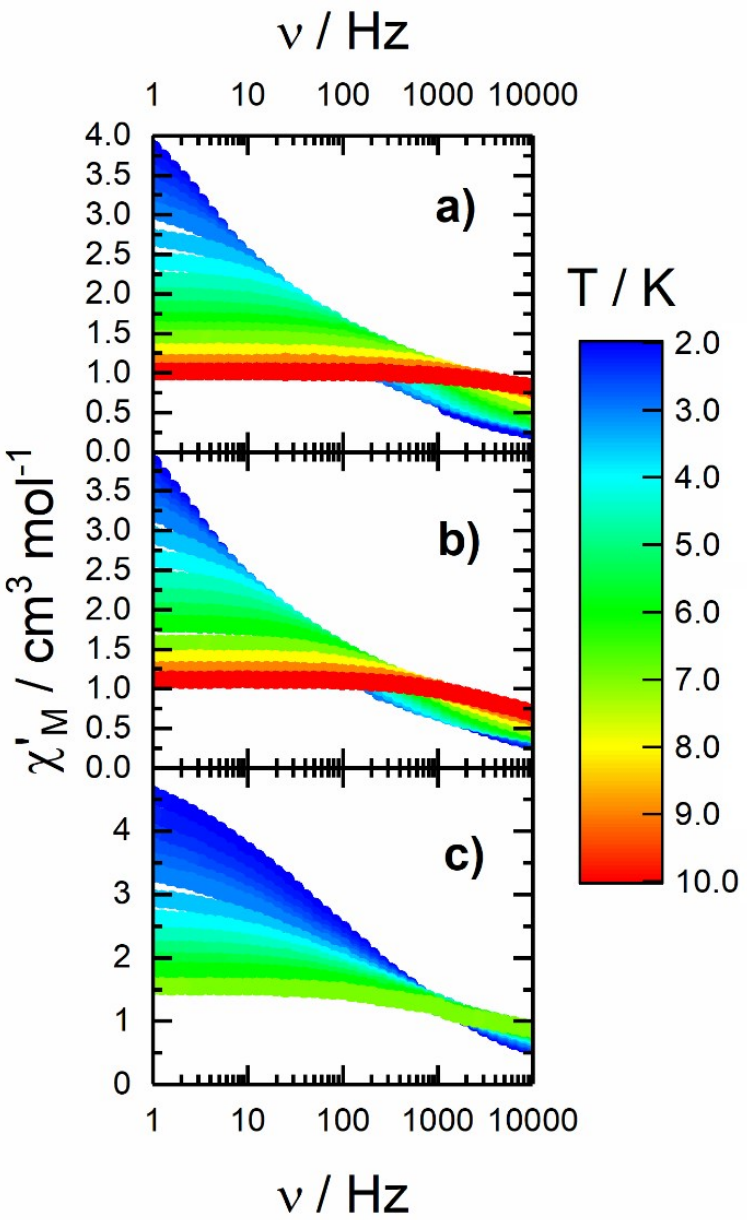

Figure S17. In-phase component of the ac magnetic susceptibility data for **[(*S*)-2]$_n$** (a), **[(*S*)-3]$_n$** (b) and **[(*S*)-4]$_n$** (c), from 2 to 10 K under 1000 Oe.

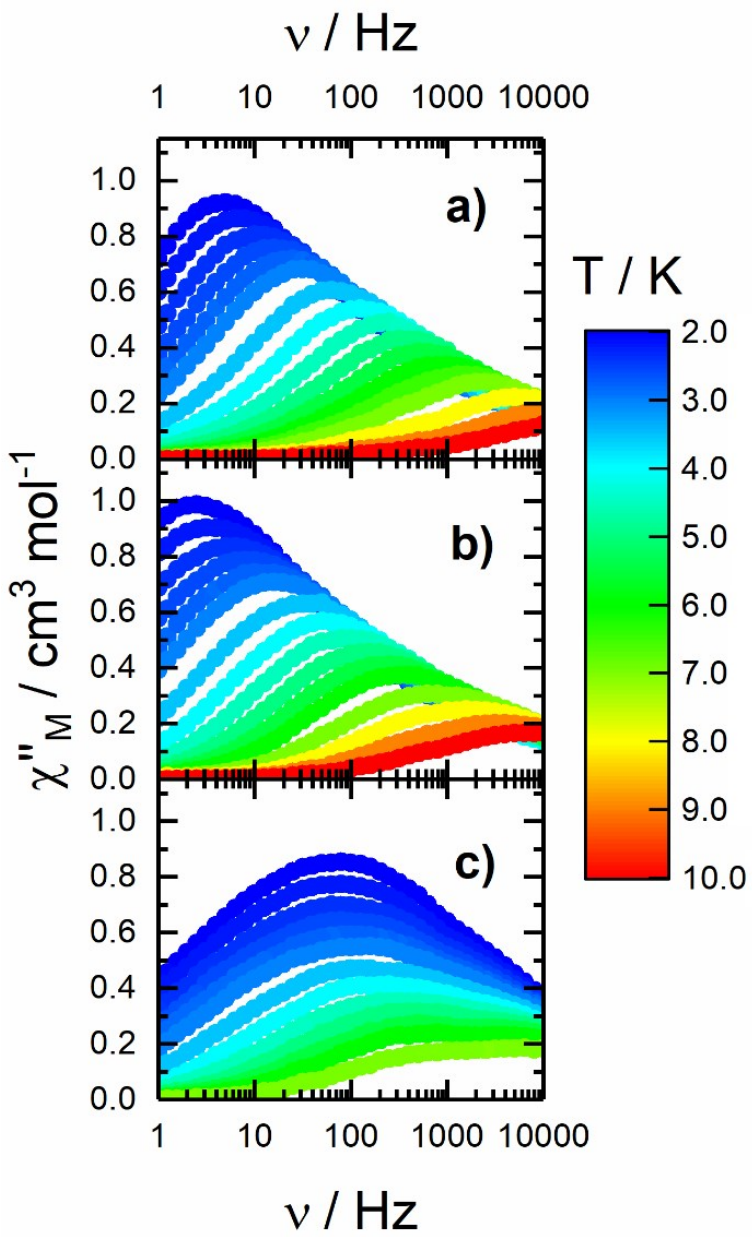

Figure S18. Frequency dependence of the out-of-phase component of the ac magnetic susceptibility data for **[(*S*)-2]$_n$** (a), **[(*S*)-3]$_n$** (b) and **[(*S*)-4]$_n$** (c), from 2 to 10 K under 1000 Oe.

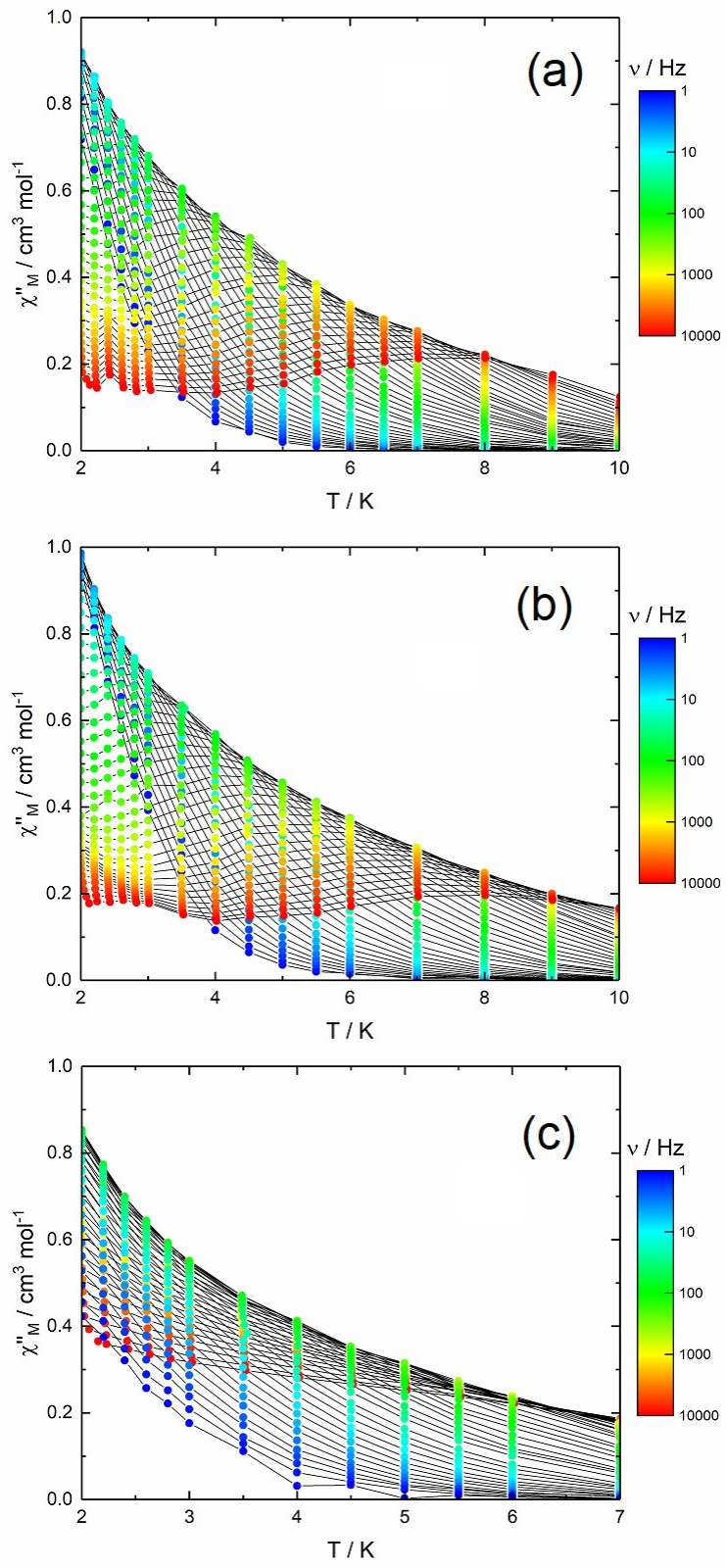

Figure S19. Thermal dependence of the out-of-phase component of the ac magnetic susceptibility data for **[(*S*)-2]$_n$** (a), **[(*S*)-3]$_n$** (b) and **[(*S*)-4]$_n$** (c), from 2 to 10 K under 1000 Oe.

Extended Debye model used for [(*S*)-2]$_n$ and [(*S*)-3]$_n$ in 1000 Oe applied field at low temperature.

$$\chi_M' = \chi_S + (\chi_T - \chi_S) \left\{ \frac{\beta\left[1 + (\omega\tau_1)^{1-\alpha_1} \sin\left(\frac{\pi}{2}\alpha_1\right)\right]}{1 + 2(\omega\tau_1)^{1-\alpha_1} \sin\left(\frac{\pi}{2}\alpha_1\right) + (\omega\tau_1)^{2(1-\alpha_1)}} + \frac{(1-\beta)\left[1 + (\omega\tau_2)^{1-\alpha_2} \sin\left(\frac{\pi}{2}\alpha_2\right)\right]}{1 + 2(\omega\tau_2)^{1-\alpha_2} \sin\left(\frac{\pi}{2}\alpha_2\right) + (\omega\tau_2)^{2(1-\alpha_2)}} \right\}$$

$$\chi_M'' = (\chi_T - \chi_S) \left\{ \frac{\beta\left[(\omega\tau_1)^{1-\alpha_1} \cos\left(\frac{\pi}{2}\alpha_1\right)\right]}{1 + 2(\omega\tau_1)^{1-\alpha_1} \sin\left(\frac{\pi}{2}\alpha_1\right) + (\omega\tau_1)^{2(1-\alpha_1)}} + \frac{(1-\beta)\left[(\omega\tau_2)^{1-\alpha_2} \cos\left(\frac{\pi}{2}\alpha_2\right)\right]}{1 + 2(\omega\tau_2)^{1-\alpha_2} \sin\left(\frac{\pi}{2}\alpha_2\right) + (\omega\tau_2)^{2(1-\alpha_2)}} \right\}$$

With χ_T the isothermal susceptibility, χ_S the adiabatic susceptibility, τ the relaxation time and α an empiric parameter which describe the distribution of the relaxation time. For SMM with only one relaxing object α is close to zero. The extended Debye model was applied to fit simultaneously the experimental variations of χ_M' and χ_M'' with the frequency ν of the oscillating field ($\omega = 2\pi\nu$). The best fitted parameters τ_1, α_1, χ_{1T}, χ_{1S}, τ_2, α_2, χ_{2T} and χ_{2S} are listed in Tables S8 and S9 with the coefficient of determination R^2. τ_1, α_1, χ_{1T}, χ_{1S} are parameters for the high frequency contribution while τ_2, α_2, χ_{2T} and χ_{2S} are for the low frequency contribution.

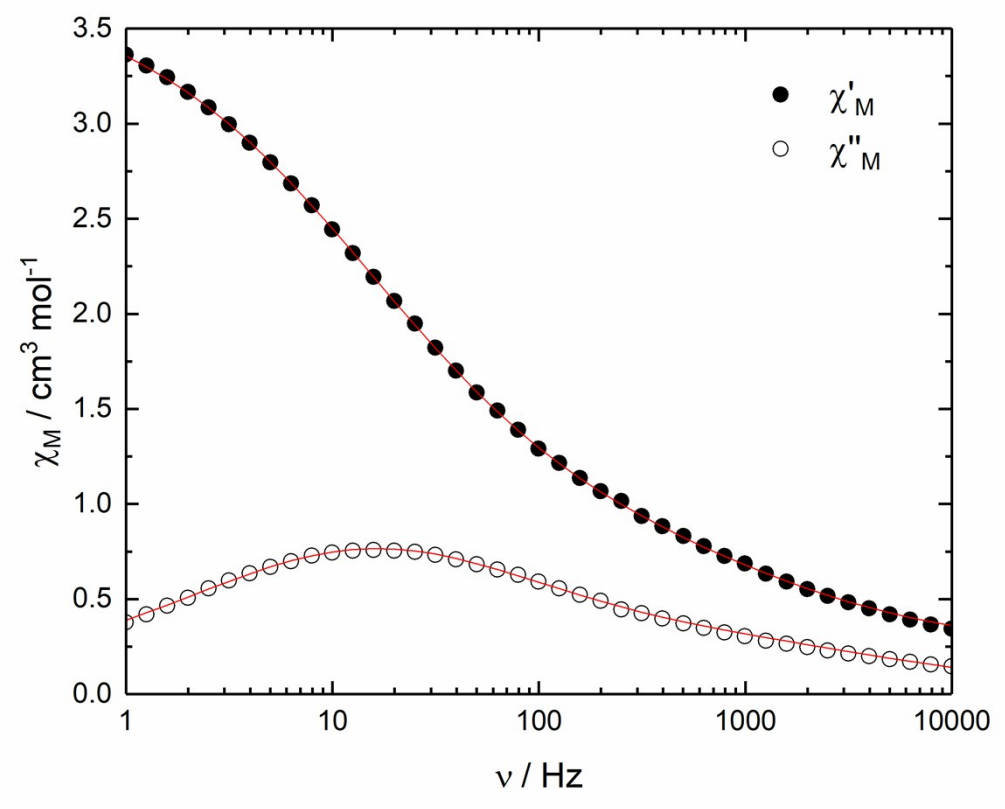

Figure S20. Frequency dependence of the in-phase (χ_M') (full circles) and out-of-phase (χ_M") (open circles) components of the ac susceptibility at 2.6 K and 1000 Oe with the best fitted curves (red lines) for **[(*S*)-2]$_n$**.

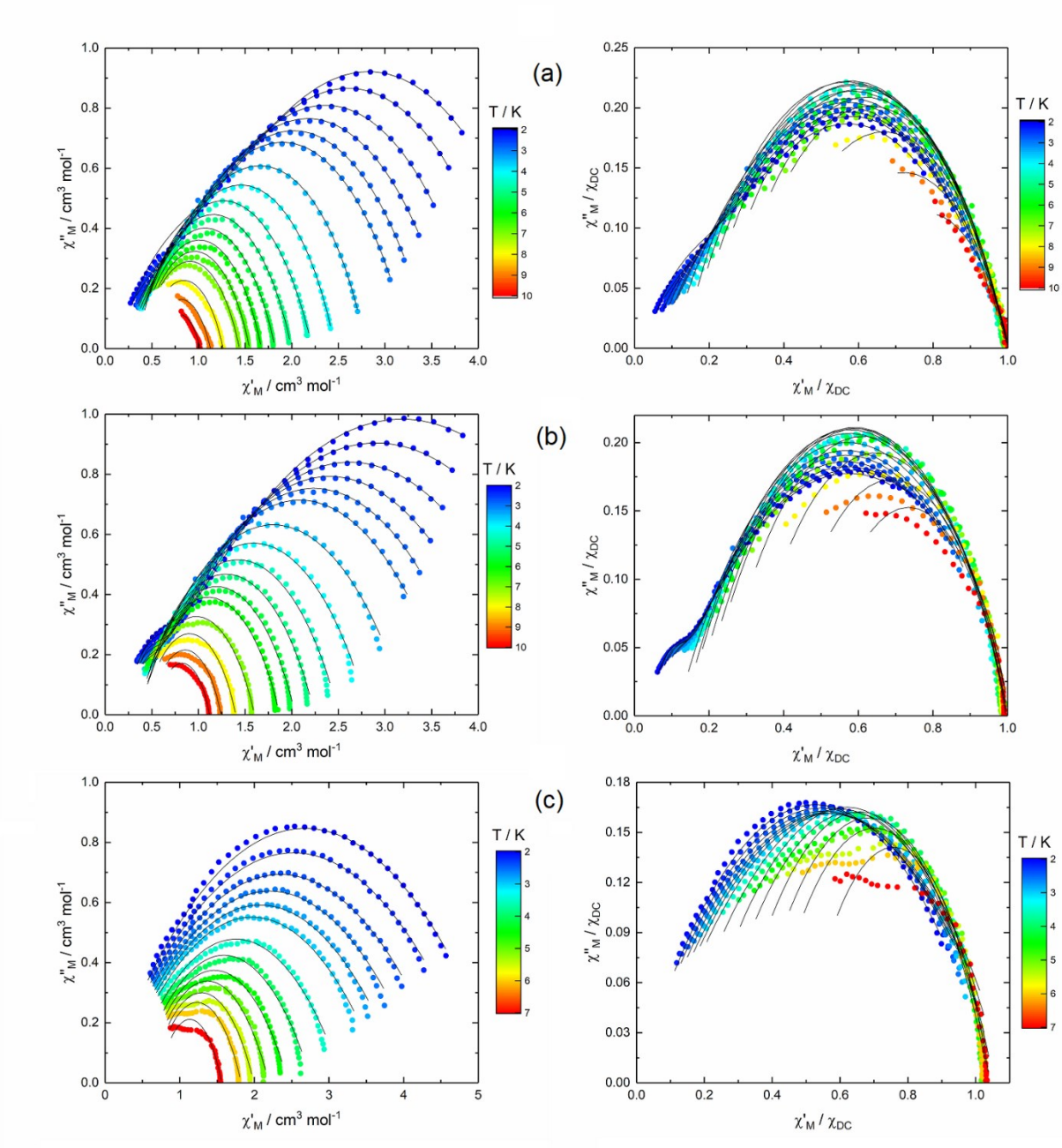

Figure S21. Cole-Cole plots (left) and normalized Cole-Cole plots (right) for **[(*S*)-2]$_n$** (a), **[(*S*)-2]$_n$** (b) and **[(*S*)-4]$_n$** (c). Full black lines are the best fits using extended Debye model detailed in the text.

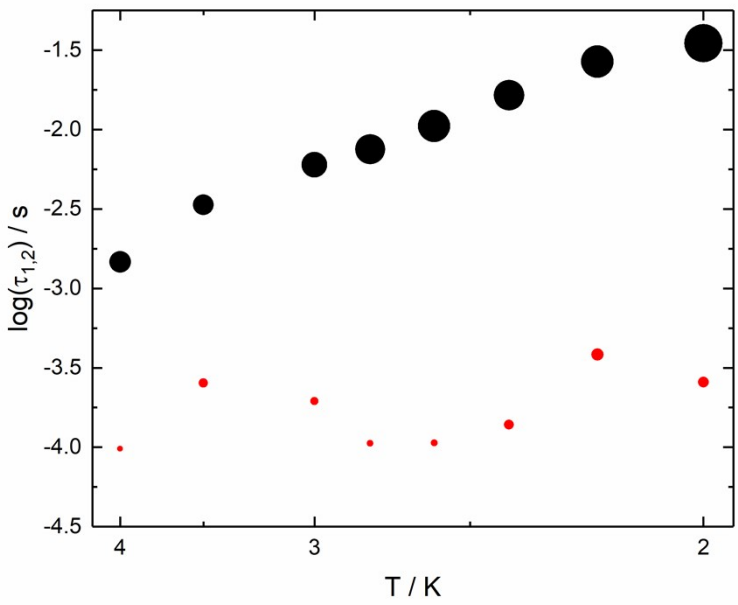

Figure S22. Arrhenius plots of the temperature dependence of the relaxation time in 1000 Oe applied magnetic field for **[(*S*)-2]$_n$** for the LF contribution (black dots) and the HF contribution (red dots). Size of the dots is representative of the ratio between the LF and HF contributions.

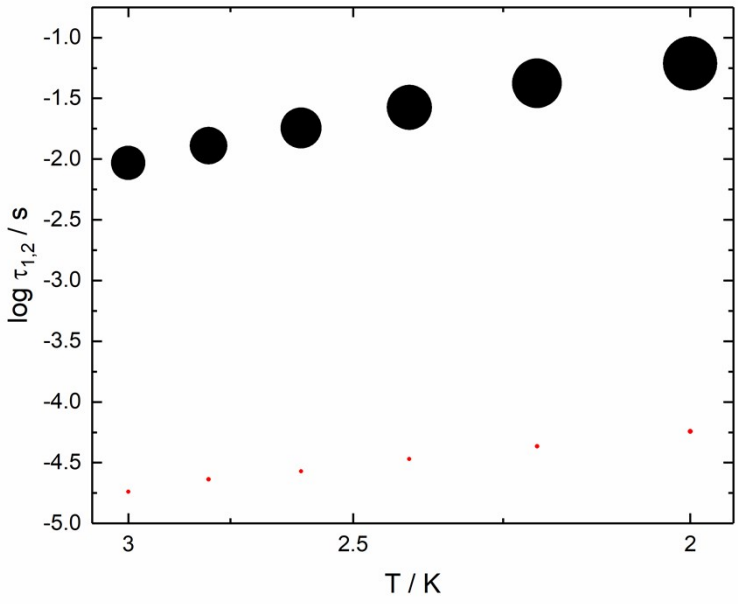

Figure S23. Arrhenius plots of the temperature dependence of the relaxation time in 1000 Oe applied magnetic field for **[(*S*)-2]$_n$** for the LF contribution (black dots) and the HF contribution (red dots). Size of the dots is representative of the ratio between the LF and HF contributions.

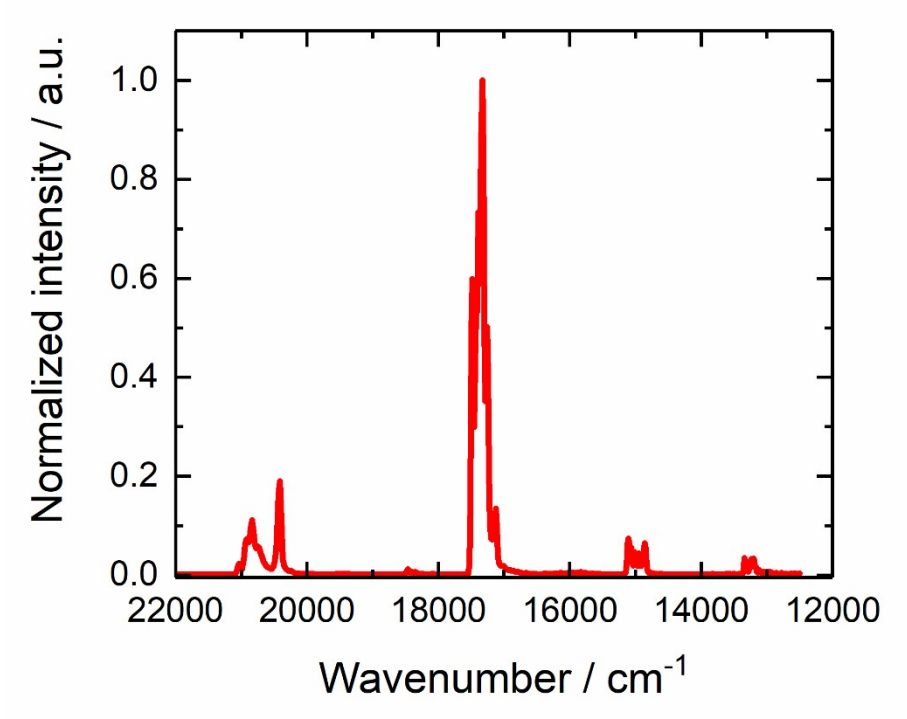

Figure S24. Emission spectrum at 10 K under an irradiation of 29400 cm^{-1} (340 nm) for **[(*S*)-3]$_n$** in solid-state.

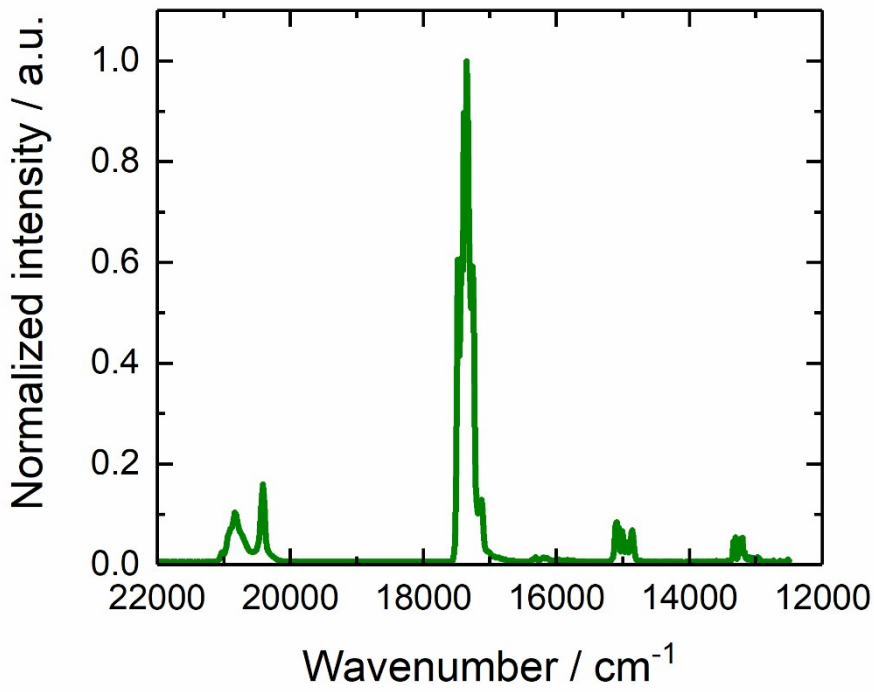

Figure S25. Emission spectrum at 10 K under an irradiation of 28570 cm^{-1} (350 nm) for **[(*S*)-4]$_n$** in solid-state.

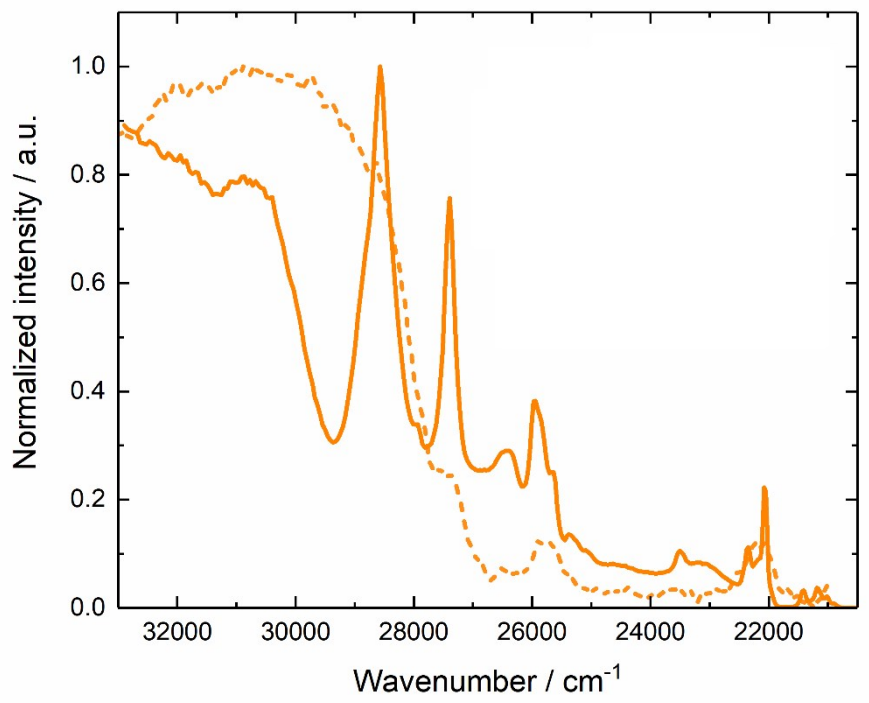

Figure S26. Excitation spectra of **[(*S*)-3]$_n$** in solid-state at room temperature (dashed orange line) and 77 K (full orange line) recorded under an excitation at 17390 cm^{-1} (575 nm).

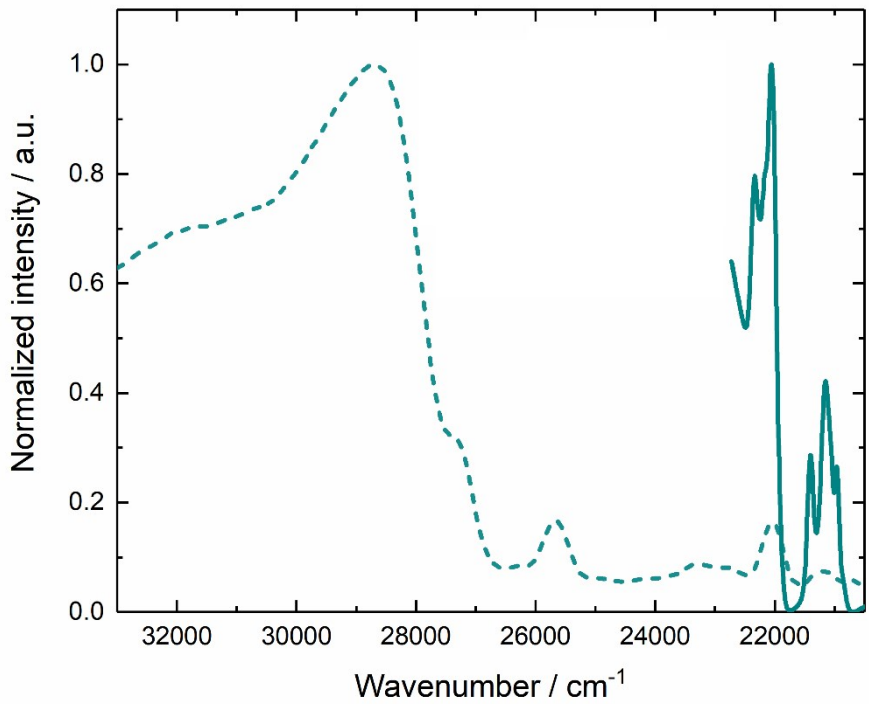

Figure S27. Excitation spectra of **[(*S*)-4]$_n$** in solid-state at room temperature (dashed green line) and 77 K (full green line) recorded under an excitation at 17390 cm^{-1} (575 nm).

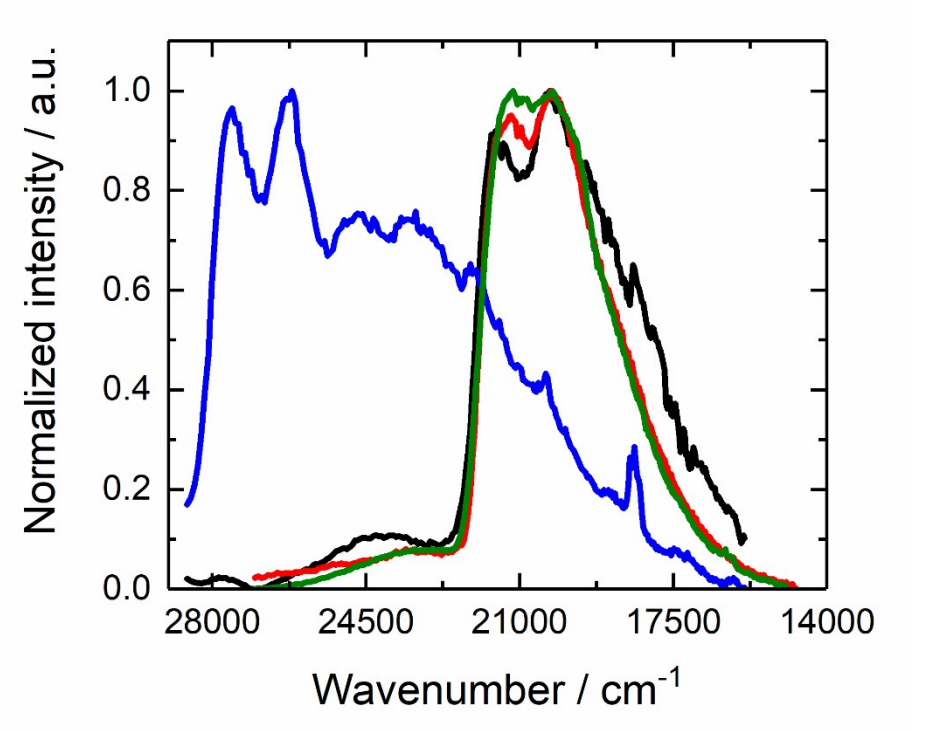

Figure S28. Phosphorescence spectra at 77 K for the Y(III) analogues of **[(*S*)-1]$_n$** (black), **[(*S*)-2]$_n$** (blue), **[(*S*)-3]$_n$** (red) and **[(*S*)-4]$_n$** (green) in the visible range for an irradiation of 29400 cm^{-1} (340 nm) in solid-state.

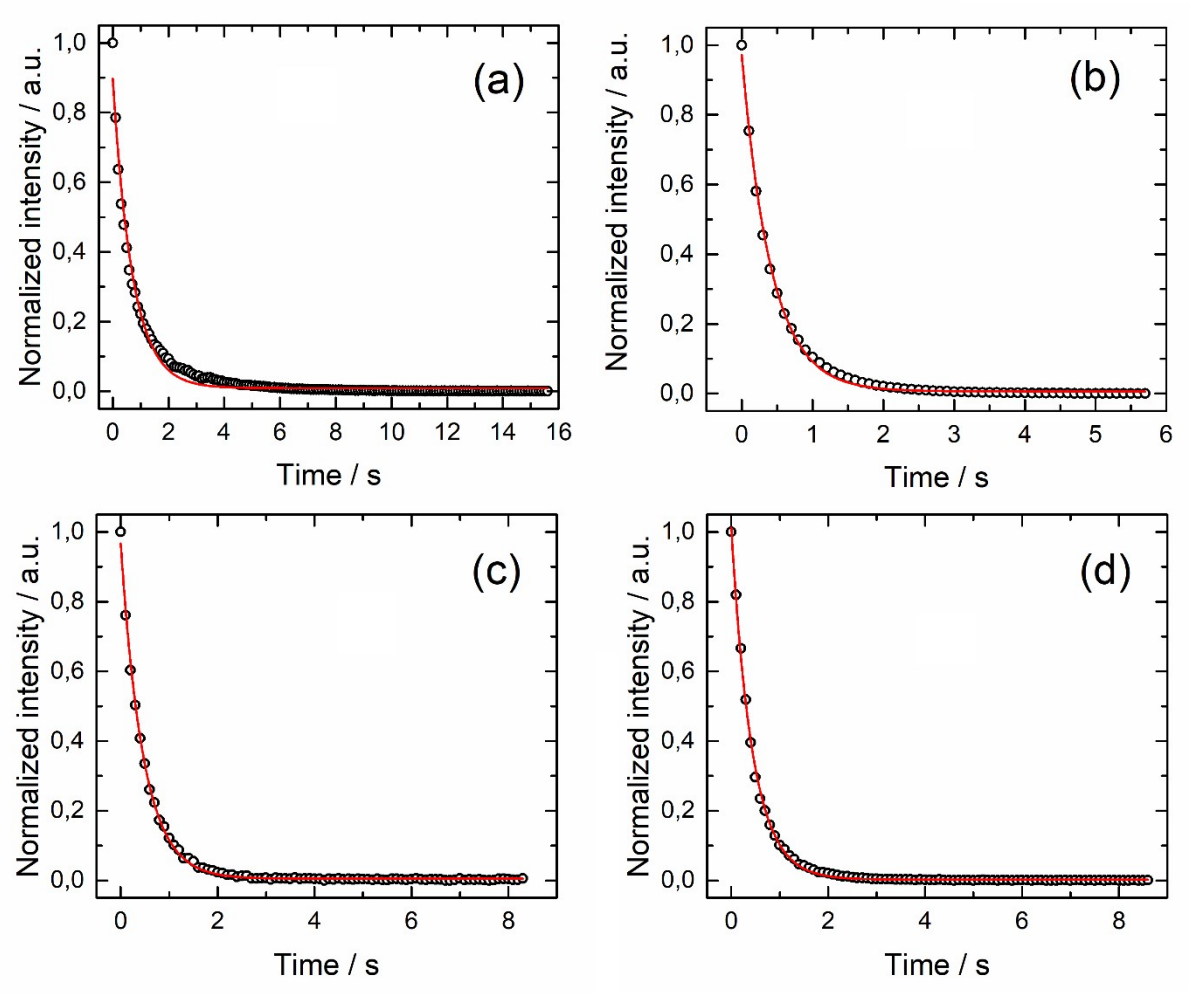

Figure S29. Phosphorescence decay for the Y(III) analogues of **[(*S*)-1]$_n$** (a), **[(*S*)-2]$_n$** (b), **[(*S*)-3]$_n$** (c) and **[(*S*)-4]$_n$** (d) recorded at 20408 cm^{-1} (490 nm) for the Y(III) analogue of **[(*S*)-1]$_n$**, 27027 cm^{-1} (370 nm) for the Y(III) analogue of **[(*S*)-2]$_n$** and 20202 cm^{-1} (495 nm) for the Y(III) analogues of **[(*S*)-3]$_n$** and **[(*S*)-4]$_n$** in solid-state at 77 K under 30303 cm^{-1} (330 nm) excitation for the Y(III) analogues of **[(*S*)-1]$_n$** and **[(*S*)-2]$_n$**; 28571 cm^{-1} (350 nm) excitation for the Y(III) analogues of **[(*S*)-3]$_n$** and **[(*S*)-4]$_n$**.

Table S1. X-ray crystallographic data for **[*S/R*-2]$_n$**, **[*S*-3]$_n$** and **[*S*-4]$_n$**.

Compound	$[Dy(hfac)_3(\mathbf{S\text{-}L^2})]_n \cdot (C_6H_{14})_2(CH_2Cl_2)_{0.5}$ **$\{[(S)\text{-}2]\cdot 2(C_6H_{14})\cdot 0.5(CH_2Cl_2)\}_n$**	$[Dy(hfac)_3(\mathbf{R\text{-}L^2})]_n \cdot (C_6H_{14})_2$ **$\{[(R)\text{-}2]\cdot 2(C_6H_{14})\}_n$**	$[Dy(hfac)_3(\mathbf{S\text{-}L^3})]_n$ **$[(S)\text{-}3]_n$**	$[Dy(hfac)_3(\mathbf{S\text{-}L^4})]_n$ **$[(S)\text{-}4]_n$**
Formula M / g.mol^{-1}	$C_{87.5}H_{68}DyF_{18}O_{14}P_2$ 1945.3	$C_{87}H_{67}DyF_{18}O_{14}P_2$ 1902.8	$C_{59}H_{43}DyF_{18}O_{14}P_2$ 1542.4	$C_{75}H_{63}DyF_{18}O_{14}P_2$ 1754.7
Crystal system	Orthorhombic	Orthorhombic	Trigonal	Tetragonal
Space group	$P2_12_12_1$ (N°19)	$P2_12_12_1$ (N°19)	P3112 (N°151)	P4122 (N°91)
Cell parameters	a = 15.8446(14) Å b = 23.038(2) Å c = 24.956(2) Å	a = 15.6774(19) Å b = 23.028(3) Å c = 25.162(3) Å	a = 13.0421(13) Å b = 13.0421 Å c = 32.276(4) Å γ = 120°	a = 18.634(4) Å b = 18.634 Å c = 26.119(5) Å
Volume / Å^3	9109.7(15)	9083.9(19)	4754.5(11)	9069(4)
Z	4	4	3	4
T / K	150(2)	150(2)	150(2)	150(2)
2θ range /°	$5.90 \leq 2\theta \leq 54.97$	$2.40 \leq 2\theta \leq 55.28$	$4.40 \leq 2\theta \leq 55.06$	$6.18 \leq 2\theta \leq 54.96$
ρ_{calc} / g.cm^{-3}	1.418	1.391	1.616	1.285
μ / mm^{-1}	0.980	0.953	1.344	0.948
Number of reflections	61598	81372	106375	53524
Independent reflections	20096	20851	7271	103016
R_{int}	0.0630	0.1017	0.0205	0.1521
$Fo^2 > 2\sigma(Fo)^2$	16241	16072	6432	5643
Number of variables	847	534	293	462
Flack parameter	0.06(2)	0.10(3)	0.023(6)	0.03(4)
R_1, ωR_2	0.0949, 0.2417	0.1518, 0.3764	0.0837, 0.2349	0.0994, 0.2219

Table S2. SHAPE analysis of the coordination polyhedra around the lanthanide in the polymeric compounds.

Compounds	Metal	$CShM_{SAPR\text{-}8}$ (square antiprism D_{4d})	$CShM_{BTPR\text{-}8}$ (biaugmented trigonal prism C_{2v})	$CShM_{TDD\text{-}8}$ (triangular dodecahedron D_{2d})
[(*S*)-2]$_n$	Dy1	0.142	2.168	2.287
[(*R*)-2]$_n$	Dy1	0.221	2.017	1.988
[(*S*)-3]$_n$	Dy1	0.310	2.076	2.091
[(*S*)-4]$_n$	Dy1	0.230	2.465	2.311

Table S3. Best fitted parameters (χ_T, χ_S, τ and α) with the extended Debye model for compound **[(*S*)-2]$_n$** at 0 Oe in the temperature range 2-8 K.

T / K	χ_T / cm^3 mol^{-1}	χ_S / cm^3 mol^{-1}	α	τ / s	R²
2	4.98683	1.09846	0.30022	2.01E-05	0.99996
2.2	4.53996	0.96466	0.30199	1.91E-05	0.99996
2.4	4.17018	0.87896	0.30393	1.86E-05	0.99998
2.6	3.86414	0.78978	0.30954	1.80E-05	0.99998
2.8	3.60085	0.66868	0.3206	1.67E-05	0.99998
3	3.36192	0.6992	0.31033	1.74E-05	0.99998
3.5	2.88742	0.64318	0.30319	1.70E-05	0.99998
4	2.53306	0.58884	0.29853	1.62E-05	0.99996
4.5	2.26644	0.50167	0.30908	1.46E-05	0.99997
5	2.04023	0.4929	0.29683	1.40E-05	0.99997
5.5	1.85474	0.44913	0.29358	1.24E-05	0.99996
6	1.70621	0.41654	0.29779	1.10E-05	0.99998
7	1.47158	0.36065	0.31681	7.79E-06	0.99998
8	1.29215	0.38523	0.32506	5.85E-06	0.99996

Table S4. Best fitted parameters (χ_T, χ_S, τ and α) with the extended Debye model for compound **[(*S*)-3]$_n$** at 0 Oe in the temperature range 2-10 K.

T / K	χ_T / cm^3 mol^{-1}	χ_S / cm^3 mol^{-1}	α	τ / s	R²
2	5.88299	0.07277	0.62095	0.03948	0.99866
2.2	5.03013	0.20859	0.57484	0.02205	0.99905
2.4	4.46807	0.22202	0.55203	0.01338	0.9988
2.6	3.99071	0.26883	0.51674	0.00864	0.99919
2.8	3.64331	0.29503	0.49057	0.00597	0.99942
3	3.37612	0.29731	0.47411	0.00426	0.99947
3.5	2.86228	0.3131	0.43554	2.07E-03	0.99963
4	2.49559	0.32252	0.40784	1.10E-03	0.99975
4.5	2.22046	0.30896	0.39424	6.25E-04	0.9997
5	1.99953	0.31765	0.37853	3.81E-04	0.99963
5.5	1.82361	0.32133	0.37486	2.44E-04	0.99971
6	1.67598	0.34463	0.36648	1.68E-04	0.99965
7	1.54807	0.37241	0.35879	1.16E-04	0.99972
8	1.43956	0.37865	0.36201	7.96E-05	0.99972
9	1.2641	0.42297	0.36899	3.76E-05	0.99973
10	1.12821	0.49336	0.39172	1.85E-05	0.99977

Table S5. Best fitted parameters (χ_T, χ_S, τ and α) with the extended Debye model for compound **[(*S*)-2]$_n$** at 2 K in the magnetic field range 200-3000 Oe.

H / Oe	χ_T / cm^3 mol^{-1}	χ_S / cm^3 mol^{-1}	τ /s	α	R^2
200	5.34365	0.19874	1.77E-05	0.3209	0.99994
400	6.00397	0.14406	2.83E-04	0.66791	0.99915
600	5.98067	0.11884	0.00979	0.67136	0.99899
800	5.65849	0.12364	0.02414	0.6384	0.99883
1000	5.37934	0.11618	0.02667	0.60659	0.99886
1200	5.05318	0.12797	0.02548	0.58878	0.99898
1400	5.25678	0.13902	0.02188	0.56874	0.99921
1600	4.93726	0.14187	0.04402	0.54758	0.99783
1800	4.63564	0.14811	0.03458	0.5323	0.99791
2000	4.34417	0.15271	0.02697	0.51805	0.99795
2200	4.07876	0.15487	0.02084	0.50488	0.99805
2400	3.82825	0.15856	0.01628	0.49494	0.99816
2600	3.59809	0.15526	0.01283	0.48713	0.99835
2800	3.38488	0.15158	0.01021	0.48338	0.99851
3000	3.1862	0.14377	0.00826	0.4829	0.99863

Table S6. Best fitted parameters (χ_T, χ_S, τ and α) with the extended Debye model for compound **[(*S*)-3]$_n$** at 2 K in the magnetic field range 200-3000 Oe.

H / Oe	χ_T / cm^3 mol^{-1}	χ_S / cm^3 mol^{-1}	τ /s	α	R^2
200	3.13626	0.90005	0.00199	0.13148	0.99982
400	4.57236	0.42183	0.01077	0.3966	0.99920
600	6.97938	0.20506	0.04126	0.62791	0.99970
800	7.11276	0.13197	0.07915	0.63434	0.99836
1000	7.21279	0.09376	0.11858	0.64092	0.99849
1200	7.12693	0.08112	0.14505	0.6433	0.99850
1400	7.01969	0.06297	0.16829	0.64906	0.99866
1600	6.85277	0.05176	0.18522	0.65495	0.99879
1800	6.77403	0 (fixed)	0.21286	0.66912	0.99890
2000	6.48608	0 (fixed)	0.21554	0.67505	0.99910
2200	6.36081	0 (fixed)	0.25512	0.68613	0.99929
2400	6.05243	0 (fixed)	0.25982	0.69375	0.99943
2600	5.78605	0 (fixed)	0.27872	0.70275	0.99945
2800	5.49398	0 (fixed)	0.29304	0.71189	0.99945
3000	5.20335	0 (fixed)	0.30995	0.72056	0.99940

Table S7. Best fitted parameters (χ_T, χ_S, τ and α) with the extended Debye model for compound **[(*S*)-4]$_n$** at 2 K in the magnetic field range 200-3000 Oe.

H / Oe	χ_T / cm^3 mol^{-1}	χ_S / cm^3 mol^{-1}	τ /s	α	R^2
200	5.15211	1.45943	6.08E-05	0.3924	0.9999
400	5.25932	0.24842	2.79E-04	0.55163	0.99988
600	5.28121	0 (fixed)	8.33E-04	0.59261	0.99989
800	5.19076	0 (fixed)	0.00156	0.59375	0.9998
1000	5.08812	0 (fixed)	0.00226	0.59668	0.99982
1200	4.98715	0 (fixed)	0.00291	0.60072	0.99986
1400	4.87559	0 (fixed)	0.00345	0.60573	0.99988
1600	4.74707	0 (fixed)	0.00382	0.60968	0.9998
1800	4.61535	0 (fixed)	0.0041	0.61421	0.99975
2000	4.49569	0 (fixed)	0.00435	0.62181	0.99977
2200	4.3549	0 (fixed)	0.00443	0.62833	0.9996
2400	4.20441	0 (fixed)	0.00446	0.63338	0.99965
2600	3.9811	0 (fixed)	0.00411	0.62891	0.99938
2800	3.91274	0 (fixed)	0.00448	0.64979	0.99943
3000	3.77056	0 (fixed)	0.00451	0.65875	0.99913

Table S8. Best fitted parameters ($\chi_{T,1}$, χ_S , τ_1, α_1, $\chi_{T,2}$, τ_2, and α_2) with the extended Debye model for compound **[(*S*)-2]$_n$** at 1000 Oe accounting for two relaxation times in the temperature range 2-4 K and for one relaxation time in the temperature range 4.5-10 K.

T / K	$\chi_{T,1}$ / cm^3 mol^{-1}	χ_S / cm^3 mol^{-1}	τ_1 / s	α_1	$\chi_{T,2}$ / cm^3 mol^{-1}	τ_2 / s	α_2	R^2
2	3.86760	0.15064	3.49300E-02	0.43534	1.08402	2.57537E-04	0.40600	0.99976
2.2	3.30470	0.16945	2.67300E-02	0.40901	1.25866	3.84271E-04	0.50916	0.99994
2.4	3.11405	0.06556	1.64700E-02	0.41832	1.00668	1.38717E-04	0.54914	0.99996
2.6	3.27021	0.22678	1.05400E-02	0.42125	0.71540	1.06640E-04	0.37707	0.99993
2.8	3.06454	0.25028	7.51000E-03	0.41175	0.68240	1.05780E-04	0.38796	0.99992
3	2.61837	0.22277	6.00000E-03	0.39099	0.86920	1.95419E-04	0.49623	0.99987
3.5	2.11902	0.28404	3.35000E-03	0.35115	0.96371	2.53307E-04	0.42260	0.99988
4	2.22141	0.33819	1.47000E-03	0.35959	0.58516	9.80544E-05	0.20930	0.99985
4.5	2.22046	0.30896	6.25294E-04	0.39424	—	—	—	0.9997
5	1.99953	0.31765	3.81079E-04	0.37853	—	—	—	0.99963
5.5	1.82361	0.32133	2.44416E-04	0.37486	—	—	—	0.99971
6	1.67598	0.34463	1.68455E-04	0.36648	—	—	—	0.99965
6.5	1.54807	0.37241	1.16087E-04	0.35879	—	—	—	0.99972
7	1.43956	0.37865	7.96390E-05	0.36201	—	—	—	0.99972
8	1.26410	0.42297	3.75632E-05	0.36899	—	—	—	0.99973
9	1.12821	0.49336	1.85135E-05	0.39172	—	—	—	0.99977
10	1.01824	0.57920	1.20060E-05	0.39099	—	—	—	0.9999

Table S9. Best fitted parameters ($\chi_{T,1}$, χ_S , τ_1, α_1, $\chi_{T,2}$, τ_2, and α_2) with the extended Debye model for compound **[(*S*)-3]n** at 1000 Oe accounting for two relaxation times in the temperature range 2-3 K and for one relaxation time in the temperature range 3.5-10 K.

T / K	$\chi_{T,1}$ / cm³ mol⁻¹	χ_S / cm³ mol⁻¹	τ_1 / s	α_1	$\chi_{T,2}$ / cm³ mol⁻¹	τ_2 / s	α_2	R^2
2	5.49010	0.19814	6.14300E-02	0.54724	0.54106	5.70629E-05	0.15059	0.99992
2.2	5.04753	0.19998	4.20600E-02	0.54544	0.48417	4.29917E-05	0.10793	0.99996
2.4	4.58678	0.22725	2.66300E-02	0.53161	0.44906	3.38742E-05	0.03284	0.99993
2.6	4.15808	0.23113	1.80300E-02	0.51137	0.44838	2.68060E-05	0.03980	0.99996
2.8	3.80167	0.23608	1.28800E-02	0.49138	0.45835	2.30314E-05	0.11359	0.99989
3	3.51877	0.22908	9.28000E-03	0.47896	0.44674	1.82509E-05	0.14545	0.99992
3.5	3.24880	0.35437	4.48000E-03	0.47558	—	—	—	0.99962
4	2.82241	0.35696	2.42000E-03	0.44735	—	—	—	0.99965
4.5	2.50657	0.33878	1.40000E-03	0.43444	—	—	—	0.99954
5	2.24675	0.34439	8.63361E-04	0.41764	—	—	—	0.99955
5.5	2.03862	0.34802	5.63566E-04	0.40464	—	—	—	0.99956
6	1.87075	0.33958	3.76012E-04	0.39911	—	—	—	0.99958
7	1.59984	0.35473	1.86353E-04	0.38437	—	—	—	0.99960
8	1.39920	0.40876	1.06272E-04	0.36498	—	—	—	0.99967
9	1.24177	0.47261	6.35764E-05	0.34999	—	—	—	0.99976
10	1.11824	0.53306	4.00388E-05	0.32489	—	—	—	0.99981

Table S10. Best fitted parameters (χ_T, χ_S, τ and α) with the extended Debye model for compound **[(*S*)-4]$_n$** at 1000 Oe in the temperature range 2-7 K.

T / K	χ_T / cm³ mol⁻¹	χ_S / cm³ mol⁻¹	α	τ / s	R^2
2	5.34602	0.00811	0.6088	0.0025	0.99976
2.2	5.02146	0.02543	0.62137	0.0023	0.99982
2.4	4.63182	0.06366	0.62466	0.00195	0.99983
2.6	4.30186	0.10807	0.62392	0.00165	0.99978
2.8	4.01087	0.14275	0.62186	0.00135	0.99981
3	3.74656	0.1886	0.61704	0.00114	0.99974
3.5	3.19865	0.3006	0.59401	7.21E-04	0.99969
4	2.77348	0.40971	0.56072	4.85E-04	0.99956
4.5	2.45563	0.47131	0.54013	3.30E-04	0.99956
5	2.19463	0.54623	0.50346	2.44E-04	0.99953
5.5	1.9924	0.59118	0.48461	1.85E-04	0.99952
6	1.82284	0.63797	0.45977	1.50E-04	0.9995
7	1.56033	0.70927	0.4129	1.02E-04	0.99947

Table S11. Energy splitting (cm^{-1}) of the $^6H_{15/2}$ multiplet state with wavefunction compositions and g factor values for each Kramer Doublet (KD) for **{[(*S*)-2]·2(C_6H_{14})·0.5(CH_2Cl_2)}$_n$, [(*S*)-3]$_n$** and **[(*S*)-4]$_n$**.

	ΔE	g_x	g_y	g_z	|15/2, M_J>
{[(*S*)-2]·2(C_6H_{14})·0.5(CH_2Cl_2)}$_n$					
GS	0	0.00	0.00	19.48	94 |±15/2> + 5 |±11/2>
ES1	64	0.03	0.08	16.92	59 |±13/2> + 17 |±9/2> + 17 |±11/2>
ES2	106	9.49	7.36	2.99	19 |±7/2> + 18 |±13/2> + 18 |±11/2>
ES3	130	7.33	5.42	0.61	25 |±7/2> + 19 |±11/2> + 15 |±9/2>
ES4	155	2.62	3.43	11.90	36 |±1/2> + 19 |±5/2> + 18 |±3/2>
ES5	181	0.21	0.49	15.39	26 |±3/2> + 25 |±1/2> + 17 |±5/2>
ES6	204	0.15	0.23	18.69	25 |±3/2> + 24 |±5/2> + 19 |±1/2>
ES7	517	0.00	0.00	19.85	26 |±9/2> + 21 |±11/2> + 21 |±7/2>
[(*S*)-3]$_n$					
GS	0	0.04	0.16	18.38	85 |±15/2> + 8 |±9/2> + 2 |±3/2>
ES1	41	3.14	4.21	12.80	33 |±13/2> + 29 |±11/2> + 12 |±1/2>
ES2	60	7.94	6.10	1.62	29 |±3/2> + 22 |±1/2> + 19 |±9/2>
ES3	89	0.09	4.99	10.05	32 |±13/2> + 27 |±5/2> + 12 |±9/2>
ES4	93	0.23	2.65	11.68	37 |±7/2> + 23 |±9/2> + 15 |±11/2>
ES5	140	1.06	2.61	15.00	31 |±5/2> + 27 |±3/2> + 26 |±7/2>
ES6	151	0.59	3.38	16.86	45 |±1/2> + 30 |±3/2> + 18 |±5/2>
ES7	473	0.00	0.00	19.84	30 |±11/2> + 26 |±9/2> + 18 |±13/2>
[(*S*)-4]$_n$					
GS	0	0.18	0.39	18.28	82 |±15/2> + 7 |±11/2> + 5 |±13/2>
ES1	23	2.09	2.54	16.58	24 |±11/2> + 20 |±1/2> + 16 |±13/2>
ES2	48	9.12	6.78	3.34	32 |±3/2> + 29 |±1/2> + 12 |±13/2>
ES3	59	3.61	3.93	4.82	27 |±3/2> + 17 |±1/2> + 16 |±9/2>
ES4	94	8.72	7.27	0.03	27 |±13/2> + 26 |±5/2> + 20 |±9/2>
ES5	116	9.64	7.58	1.47	25 |±7/2> + 21 |±9/2> + 17 |±3/2>
ES6	135	2.55	3.95	14.45	38 |±7/2> + 32 |±5/2> + 15 |±3/2>
ES7	473	0.00	0.00	19.83	33 |±11/2> + 24 |±9/2> + 22 |±13/2>

Table S12. TD-DFT calculated absorption energies and main compositions of the low-lying electronic transitions for (*S*)-L[1]. H and L represent the HOMO and LUMO, respectively. The theoretical values are evaluated at the PCM(CH_2Cl_2)-PBE0/SVP level of approximation.

Energy exp (cm^{-1})	Energy theo (cm^{-1})	Osc.	Transition
31000	32804	0.14	H→L (96%)
34500	35643 36360	0.05 0.06	H→L+2 (25%) H-1→L+1 (96%) H-4→L (27%)
38200	41387	0.06	H-1→L+4 (33%) H→L+2 (41%)
43000	45410 45725	0.70 0.35	H-1→L+6 (19%) H-8/-9→L+1 (41%)

Table S13. TD-DFT calculated absorption energies and main compositions of the low-lying electronic transitions for (*S*)-L[2]. H and L represent the HOMO and LUMO, respectively. The theoretical values are evaluated at the PCM(CH_2Cl_2)-PBE0/SVP level of approximation.

Energy exp (cm^{-1})	Energy theo (cm^{-1})	Osc.	Transition
31100	31443	0.12	H-2→L (41%) H-3→L+1 (48%)
33100	31493	0.31	H-2→L+1 (44%) H-1→L (48%)
34000	31729 32630	0.13 0.03	H→L/+2 (31/61%) H→L/+2 (31/61%)
36500	36936 + 36971	0.06 + 0.04	H-4→L+3(30%) H-3→L+4(27%) H-2→L+5(18%) H-4→L+4 (30%) H-3→L+3(31%)
38200	40037 + 40481	0.14 + 0.13	H-6/-7→L (13/10%) H-8/-9→L+1(8/9%) H-6→L+4(10%) H-8→L+3(8%) H-9→L+1 (12%) H-7→L(15%) H-4→L+4(11%) H-3→L+3 (9%)
43500	/	/	/

Table S14. TD-DFT calculated absorption energies and main compositions of the low-lying electronic transitions for (*S*)-L^3. H and L represent the HOMO and LUMO, respectively. The theoretical values are evaluated at the PCM(CH_2Cl_2)-PBE0/SVP level of approximation.

Energy exp (cm^{-1})	Energy theo (cm^{-1})	Osc.	Transition
36500	40560 40768	0.04 0.02	H→L (63%) H-1→L (61%)
37500	43465 43638	0.03 0.02	H-2→L+1 (32%) H-3→L+7 (13%) H-4→L (23%) H→L (19%)
38500	45844 46251 46609	0.04 0.06 0.04	H→L+3 (43%) H-1→L+2 (48%) H→L+4 (42%)
43000	48847 48962 49237	0.04 0.04 0.04	H-4→L+3(30%) H-7→L+1(20%) H-3→L+5(15%) H-3→L+5 (32%)

Table S15. TD-DFT calculated absorption energies and main compositions of the low-lying electronic transitions for (*S*)-L^4. H and L represent the HOMO and LUMO, respectively. The theoretical values are evaluated at the PCM(CH_2Cl_2)-PBE0/SVP level of approximation.

Energy exp (cm^{-1})	Energy theo (cm^{-1})	Osc.	Transition
38300	39268	0.06	H-3→L (43%)
40300	40332 40362	0.02 0.03	H-8→L+1 (29%) H-7→L (41%)
41600	41044 41115	0.14 0.38	H-1/-5→L+1 (49%)
43700	45602 45670 46198 46256	0.26 0.22 0.12 0.13	H-1→L+3/+4(38%) H-3→L(10%) H/-2→L+3(21%) H-7→L+2 (16%) H-3→L+3/+4 (41%) H-2/-4→L+3/+4 (42%)

Table S16. DFT calculated relative energy of the low-lying triplet state T_1 with respect to the S_0 ground state of L^2, L^3 and L^4.

Ligands	T_1 relative energy (cm^{-1})
(*S*)-L^2	20813
(*S*)-L^3	27587
(*S*)-L^4	25633